HHS Public Access

Author manuscript

Psychiatry Res. Author manuscript; available in PMC 2016 November 30.

Published in final edited form as:

Psychiatry Res. 2015 November 30; 234(2): 265–271. doi:10.1016/j.pscychresns.2015.10.002.

Predictive classification of pediatric bipolar disorder using atlas-based diffusion weighted imaging and support vector machines

Benson Mwangi[#a,*], **Mon-Ju Wu**[#a], **Isabelle E. Bauer**[a], **Haina Modi**[a], **Cristian P. Zeni**[a], **Giovana B. Zunta-Soares**[a], **Khader M Hasan**[b], and **Jair C. Soares**[a]

[a]UT Center of Excellence on Mood Disorders, Department of Psychiatry and Behavioral Sciences, UT Houston Medical School, Houston, TX, USA

[b]Department of Diagnostic & Interventional Imaging, The University of Texas Health Science Center at Houston, Houston, TX, USA

[#] These authors contributed equally to this work.

Abstract

Previous studies have reported abnormalities of white-matter diffusivity in pediatric bipolar disorder. However, it has not been established whether these abnormalities are able to distinguish individual subjects with pediatric bipolar disorder from healthy controls with a high specificity and sensitivity. Diffusion-weighted imaging scans were acquired from 16 youths diagnosed with DSM-IV bipolar disorder and 16 demographically matched healthy controls. Regional white matter tissue microstructural measurements such as fractional anisotropy, axial diffusivity and radial diffusivity were computed using an atlas-based approach. These measurements were used to `train' a support vector machine (SVM) algorithm to predict new or `unseen' subjects' diagnostic labels. The SVM algorithm predicted individual subjects with specificity = 87.5%, sensitivity = 68.75%, accuracy = 78.12%, positive predictive value = 84.62%, negative predictive value = 73.68%, area under receiver operating characteristic curve (AUROC) = 0.7812 and chi-square p-value = 0.0012. A pattern of reduced regional white matter fractional anisotropy was observed in pediatric bipolar disorder patients. These results suggest that atlas-based diffusion weighted imaging measurements can distinguish individual pediatric bipolar disorder patients from healthy

[*]Corresponding author: Department of Psychiatry & Behavioral Sciences, The University of Texas Health Science Center, 1941 East Road, Houston, TX 77054, USA. Tel.: +1 7134862624; Fax: +1 7134862553, benson.irungu@uth.tmc.edu.

Contributors

Benson Mwangi – Neuroimage data pre-processing, implementation of atlas-based approach, implementation of support vector machines, data interpretation and manuscript preparation.

Mon-Ju Wu - Neuroimage data pre-processing, implementation of atlas-based approach, implementation of support vector machines, data interpretation and manuscript preparation.

Isabelle E. Bauer – Neuroimaging data pre-processing and manuscript preparation.

Haina Modi – Data management and manuscript preparation.

Cristian P. Zeni – Data interpretation and manuscript preparation.

Giovana B. Zunta-Soares – Data collection, management and manuscript preparation.

Khader M. Hasan – Data interpretation, implementation of atlas-based approach and manuscript preparation

Jair C. Soares - Data collection, Data interpretation, manuscript preparation

All other authors report no conflicts of interest to declare.

controls. Notably, from a clinical perspective these findings will contribute to the pathophysiological understanding of pediatric bipolar disorder.

Keywords

Pediatric bipolar disorder; Diffusion weighted imaging; Support vector machines; Machine learning; Pattern classification

1. Introduction

Bipolar disorder is a severe and disabling neuropsychiatric disorder affecting approximately 1 – 2% of youths in the general population (Jonas et al., 2003; Kupfer, 2005; Merikangas et al., 2012). There is converging evidence that early onset bipolar disorder follows a more severe course leading to poorer long-term clinical outcomes with nearly a third of these patients attempting suicide (Goldstein et al., 2005; Post et al., 2010). These facts translate into a high medical and socio-economic burden - which further highlights the need to elucidate the etiology of pediatric bipolar disorder (PBD).

White matter tissue plays an important role in connecting multiple brain regions – many of which are tasked in performing specific roles such as executive functioning, memory and emotion regulation. Abnormalities in these systems have previously been implicated in the etiology of PBD (Passarotti et al., 2010). Diffusion tensor imaging (DTI) is a neuroimaging technique used to characterize microstructural characteristics of white-matter tissue *in vivo* and widely used in studying white matter tissue characteristics in psychiatric disorders. In particular, fractional anisotropy (FA), radial diffusivity (RD) and axial diffusivity (AD) are three DTI-derived metrics used to probe white matter tissue water directionality and diffusivity (Johansen-Berg and Behrens, 2013; Pierpaoli et al., 1996). Briefly, higher FA values (0 - minimum, 1 – maximum) depict tissue watter diffusion along one direction while restricted in other directions. Both human and animal studies have reported increased white matter FA during postnatal brain development – a period which is associated with increased myelination (Johansen-Berg and Behrens, 2013; Kochunov et al., 2012; Mori et al., 2001; Mwangi et al., 2013; Pierpaoli et al., 1996). In comparison, AD – which represents the eigenvalue of the principal eigenvector from the diffusion tensor (also referred to as parallel diffusion) has previously been associated with axonal degeneration (Song et al., 2003). Lastly, RD – which represents average eigenvalues from the second and third eigenvectors of a diffusion tensor (also referred to as perpendicular diffusion) has been associated with myelin damage in animal models (Song et al., 2002; Johansen-Berg and Behrens, 2013). As a result, these measurements have recently been used to investigate white matter microstructural characteristics with converging evidence indicating altered FA patterns in PBD. Specifically, patterns of reduced FA values have been reported in the anterior cingulate, corpus callosum and superior frontal white matter in PBD patients as compared to healthy controls (Gönenç et al., 2010; James et al., 2011; Gao et al., 2013; Adler et al., 2014).

Although the above studies have undeniably contributed to the understanding of white matter abnormalities in PBD – they have largely established average *group-level* differences

between PBD and healthy controls groups. Consequently, findings have not been translated into clinical practice. Noticeably, a major first step in achieving this goal is to establish predictive utility (high sensitivity and specificity) of DTI measurements in identifying individual patients with PBD from healthy controls. Consequently, in this study we utilized atlas-based FA, AD and RD measurements coupled with a multivariate support vector machine (SVM) algorithm (Vapnik, 1998) to predict individual PBD patients from healthy controls.

In conclusion, the primary objective of this study was to investigate the utility of DTI-derived measures (e.g. FA) in predicting individual PBD patients from healthy controls using a SVM algorithm. A secondary objective was to elucidate anatomical regions most relevant in distinguishing individual PBD patients from healthy controls.

2. Methods

2.1. Subjects

Study approval was obtained from the local institutional review board (IRB) at the University of North Carolina at Chapel Hill (UNC) and written informed assent and consent obtained from all subjects and parents/guardians. Study participants included 16 children and adolescents with DSM-IV (Diagnostic and Statistical Manual, 4^{th} edition) diagnosis for bipolar disorder and 16 healthy controls matched for gender, age, pubertal status, ethnicity, years of education and handedness as shown in Table 1. Patients' exclusion criteria included; substance abuse within the past six months and general medical problems. The inclusion criteria for healthy controls included the absence of a history of any psychiatric disorders and substance abuse or neurologic disorders and a history of any Axis I psychiatric disorders in first degree relatives. Exclusion criteria for both patient and healthy control groups included head injury with loss of consciousness, presence of metallic objects in the body, family history of hereditary neurological disorders, and pregnancy.

2.2. Magnetic resonance imaging protocol

DWI scans were acquired using a 3.0 T Siemens Allegra scanner using a spin echo-planar imaging protocol with the following acquisition parameters. Echo time = 79 ms, repetition time = 9200 ms, slice thickness = 2 mm, voxel size = 2 mm, image matrix = 104×128 with 21 diffusion encoding directions, b-value = 1000 s/mm^2 and one non-diffusion weighted volume. At the same time, T_1-weighted scans were acquired using a three-dimensional magnetization prepared rapid gradient echo (3D MPRAGE) protocol with the following parameters. Repetition time (TR) = 1750 ms, echo time (TE) = 4.38 ms, flip angle = 8°, Slice thickness = 1 mm, matrix size = 256×208 and voxel size = 1 mm.

2.3. Image pre-processing

All scans (DWI and T_1-weighted) were visually inspected to rule out gross artefacts including any `ghosting' effect. DWI scans were pre-processed using the FMRIB software package (FSL) version 5.0.7 (Smith, 2002) as described in the following four steps: 1) Correction for `eddy currents' using the `*eddy_correct*' routine in FSL and discussed in detail elsewhere (Johansen-Berg and Behrens, 2013). 2) Removal of skull and non-brain tissue

using FSL's brain extraction tool (BET)(Smith, 2002). 3) Calculation and fitting of a diffusion tensor at every voxel using the `*dtifit*' routine in FSL and discussed in detail elsewhere (Johansen-Berg and Behrens, 2013). 4) Estimation of FA, AD and RD volumes for each subject to facilitate the ensuing atlas-based regional measurement extraction.

T_1-weighted scans were automatically segmented using the freesurfer software library version 5.3.0 (http://surfer.nmr.mgh.harvard.edu/) (Fischl, 2012). Brain white matter tissue was parcellated using an automated technique utilizing morphometric landmarks and gray / white matter boundary information as explained in detail elsewhere (Salat et al., 2009). This process resulted in 68 white matter tissue atlas parcellations which included caudal anterior cingulate, caudal middle frontal, superior temporal, entorhinal, parahippocampal and paracentral white matter among other regions as listed in Table S1 of Supplementary Materials. These white matter parcellations have been used successfully in other neuroimaging studies (including pediatric) (Salat et al., 2009; Tamnes et al., 2010; Hasan et al., 2011, 2012).

2.4. Image co-registration

Image registration routines were implemented to co-register T_1-weighted and DWI volumes and subsequently extract regional FA, AD and RD in the T_1-weighteed derived white matter parcellations. Specifically, the FMRIB's linear registration tool (FLIRT) as implemented in FSL (Smith, 2002) was used with non-diffusion weighted (b=0) and Freesurfer white-matter parcellations as `source' and `target' volumes, respectively, as shown in Fig. 1a. FLIRT was executed using 12 degrees of freedom with a correlation ratio cost function resulting into an affine transformation matrix. The resulting transformation matrix was applied to other diffusion weighted volumes (FA, RD and AD). Lastly, average FA, RD and AD values for each anatomical region as defined through the T_1-weighted Freesurfer white matter parcellations were computed and used in the ensuing machine learning analyses. This resulted into an input data matrix of 68 anatomical features from both hemispheres with 32 subjects in total (16 PBD patients, 16 healthy controls; Table 1).

2.5. Machine learning

Briefly, we describe the SVM learning process. Specifically, given example training data (e.g. FA) with corresponding diagnostic labels (healthy controls +1, PBD −1), the SVM algorithm identifies an `optimal' boundary or hyperplane able to separate Healthy controls from patients. The identified or `learnt' boundary is used during the algorithm testing stage to categorize new or `unseen' subjects' into either patient or healthy control categories. For a detailed mathematical formulation of the SVM algorithm the reader is pointed elsewhere. (Vapnik, 1998; Mwangi et al., 2012; Orrù et al., 2012; Johnston et al., 2013, 2014). In the current study, the SVM algorithm was implemented in Matlab (The Mathworks, Inc., Natick, MA) using a SVM toolbox (Schwaighofer, 2001) and in house custom software. Consequently, SVM was `trained' using atlas-based DWI measurements (e.g. FA) to identify a *hyperplane* or boundary that optimally separates PBD patients from healthy controls. The identified *hyperplane* was used in the algorithm `testing' stage to predict `unseen' subjects' diagnostic labels. To establish SVM's generalization ability to `novel' or previously `unseen' DWI measurements – training and testing data were separated using a leave-one-out cross-

validation (LOOCV) approach as shown in Fig. 1b. This cross-validation approach involved training a SVM algorithm with all subjects but one and the remaining subject was used for algorithm testing. The LOOCV approach is optimal when the study sample size is small as it allows the algorithm `training' sub-sample to be maximized (Klöppel et al., 2012; Wu et al., 2015). Importantly, as SVM is a kernel learning algorithm, we evaluated utility of three of the most used kernel functions in neuroimaging (linear, polynomial and radial basis function –RBF). A *grid-search* procedure was used to select Kernel function and SVM regularization parameters using training data only to avoid circularity or *double-dipping* (Kriegeskorte et al., 2009). The SVM with a linear kernel was used with a fixed regularization parameter (C=1) as it has previously been shown that varying this parameter with a linear kernel does not improve prediction accuracy (Wu et al., 2015). Subjects' actual labels and SVM predicted labels following LOOCV were compared through a `confusion matrix' and prediction accuracy, specificity, sensitivity, positive predictive value (PPV), negative predictive value (NPV), area under receiver operating characteristic curve (AUROC) and the chi-squire *p*-value recorded. These parameters are described in detail elsewhere (Misaki et al., 2010; Johnston et al., 2013; Mwangi et al., 2014a; Mwangi et al., 2014b). The chi-squire significance was defined as ($p<0.05$). Lastly, patterns of anatomical regions weighted highly by the linear SVM algorithm and `most relevant' in distinguishing PBD patients from healthy controls were identified and reported.

3. Results

PBD patients and healthy control groups were matched based on gender, age, years of education, ethnicity and pubertal status as summarized in Table 1. The SVM algorithm trained with a linear kernel function and FA values performed best with accuracy = 78.12 % sensitivity = 68.75 % specificity =87.5 %, PPV = 84.62 %, NPV = 73.68 % and AUROC =0.781 %. A `confusion matrix' and ROC curve used to generate these prediction results are shown in Fig. 2. These predictions were significant with chi-square *p*-value =0.0012. Predictions from AD and RD were both above chance level (>50%) at (59.38% and 56.25%) respectively although the chi-squire *p*-values were not significant ($p=0.24$, $p=0.48$). A summary of prediction results from other measurements (RD and AD) is shown in Table 2. In addition, prediction accuracy results with other non-linear SVM kernel functions (2^{nd} order polynomial and Gaussian radial basis function) were both at chance level 53.2 % and 53.2 %, respectively. The `most relevant' anatomical regions (high SVM weighting factors) in predicting PBD patients from healthy controls included; Left banks of the superior temporal sulcus, left frontal pole, left Parahippocampal gyrus, left transverse temporal gyrus, right temporal pole, left anterior cingulate gyrus, and right transverse temporal gyrus. These anatomical regions are shown in Fig. 3a. FA values were consistently reduced in the PBD patient group as compared to healthy controls as a shown in Fig. 3b. A list of top most relevant anatomical regions is shown in Table 3. A detailed tabulation of all anatomical regions and their SVM relevance is shown in Table S1 of Supplementary Materials. Results suggest FA can be used as an accurate signature able to identify PBD patients at an individual subject level.

4. Discussion

In this study, we report prediction of individual PBD patients from healthy controls using DWI derived FA values with 78.12% accuracy. These predictions were significant (chi-square p-value <0.05) and within the range of prediction results previously reported in neuroimaging machine learning studies (Orrù et al., 2012). This is a significant advance as previous DWI studies in PBD have largely reported *group-level* differences on DWI measurements (e.g. FA) (Frazier et al., 2007; James et al., 2011; Gao et al., 2013; Adler et al., 2014). Markedly, machine learning studies as presented here have recently been recognized as possible avenues of translating psychiatric research into clinical research as they are able to make inferences at an individual subject level (Krystal and State, 2014). Most notably, these studies utilize cross-validation steps (e.g. leave-one-out) to avoid circularity and establish generalization ability from previously unseen subjects.

The most relevant anatomical regions in distinguishing patients from controls included; Left banks of the superior temporal sulcus, left frontal pole, left parahippocampal gyrus, left transverse temporal gyrus, right temporal pole, left anterior cingulate gyrus and right transverse temporal gyrus (see Table 3). These regions indicated consistent patterns of reduced FA in PBD patients as compared with healthy controls. This is in line with converging evidence from *in vivo* and histological studies in animal models associating low anisotropy in white matter with abnormal myelination (Mori and Zhang, 2006).

The left bank of the superior temporal sulcus (STS) is located within the temporal lobe, adjacent to the superior and middle temporal gyri and associated with extracting socially relevant cues such as social perception, audio-visual integration and face processing (Hein and Knight, 2008). In addition, STS is heavily inter-connected with several other brain regions such as lateral prefrontal cortex and ventral/medial frontal cortices (Hein and Knight, 2008). Patterns of FA abnormalities in STS may contribute to disturbances in affect processing circuity resulting into mood abnormalities (Bruno et al., 2008). Indeed, alterations of STS in PBD have also been reported in functional neuroimaging studies (Pavuluri et al., 2007). The frontal pole is the most rostral part of the brain and considered as part of Brodmann area 10 (BA10) as well as the prefrontal cortex. The frontal pole is primarily tasked with cognition, emotion processing and working memory with a recent study suggesting to be subdivided into two components (frontal pole1, frontal pole2) each with unique tasks (Bludau et al., 2014). Markedly, research with lesion patients have established that brain lesions close to the left frontal pole are related to severity of depressive symptoms – suggesting alterations of the left prefrontal cortex are associated with depression (Harmon-Jones et al., 2008). A recent study reported altered amygdala-frontal pole connectivity in PBD patients as compared with healthy controls (Stoddard et al., 2015). In addition, we observed reduced FA values in both left and right parahippocampal gyrus and transverse temporal gyrus. The parahippocampal gyrus is part of the limbic system which plays a critical role in emotion regulation and several studies have linked abnormal connectivity in this system with dysfunction in PBD (Barnea-Goraly et al., 2009). Altogether, these results suggest white matter related abnormalities in brain regions associated with emotion processing, cognition and working memory.

Potential limitations of the current study should be noted. First, the sample size was relatively small with a total of 32 subjects in both patient and control groups. However, the machine learning approach allowed us to utilize a cross-validation approach (LOOCV) and robustly establish the generalization ability of the algorithm to previously `unseen' subjects data. Nonetheless, these findings should be replicated in a larger sample size before being considered for a clinical application. Second, six PBD patients were currently taking psychotropic medications – which is a reflection of standard clinical practice and psychiatric research (see Table S3 of Supplementary Materials). However, these findings should be established in a medication naïve patient sample to avoid medication confounds. Third, PBD patients included in this study reported comorbidities with other disorders such as attention deficit hyperactivity disorder (ADHD) and oppositional defiant disorder (ODD). Prediction results from nonlinear kernel functions (2nd order polynomial and Gaussian radial basis function) did not exceed chance level accuracy (53.2%). This could be attributed to a non-linear algorithm `overfitting' – where an overly complex model is unable to generalize well to novel subjects' data. However, the potential risk of overfitting warrants further investigation in future studies. In conclusion, we have presented a novel approach of classifying PBD patients from healthy controls using atlas-based DWI measurements and support vector machines. These results will contribute to the mechanistic understanding of PBD.

Supplementary Material

Refer to Web version on PubMed Central for supplementary material.

Acknowledgments

The research reported was supported in part by NIMH grant R01 085667, the Dunn Foundation, and the Pat Rutherford, Jr. Endowed Chair in Psychiatry to JCS. JCS has participated in research funded by Forest, Merck, BMS, GSK and has been a speaker for Pfizer and Abbott.

References

Adler, CM.; Adams, J.; DelBello, MP.; Holland, SK.; Schmithorst, V.; Levine, A.; Jarvis, K.; Strakowski, SM. Evidence of white matter pathology in bipolar disorder adolescents experiencing their first episode of mania: a diffusion tensor imaging study. 2014. In preparation

Barnea-Goraly N, Chang KD, Karchemskiy A, Howe ME, Reiss AL. Limbic and corpus callosum aberrations in adolescents with bipolar disorder: a tract-based spatial statistics analysis. Biological Psychiatry. 2009; 66:238–244. [PubMed: 19389661]

Bludau S, Eickhoff S, Mohlberg H, Caspers S, Laird A, Fox P, Schleicher A, Zilles K, Amunts K. Cytoarchitecture, probability maps and functions of the human frontal pole. Neuroimage. 2014; 93:260–275. [PubMed: 23702412]

Bruno S, Cercignani M, Ron MA. White matter abnormalities in bipolar disorder: a voxel-based diffusion tensor imaging study. Bipolar Disorders. 2008; 10:460–468. [PubMed: 18452442]

Fischl B. FreeSurfer. Neuroimage. 2012; 62:774–781. [PubMed: 22248573]

Frazier JA, Breeze JL, Papadimitriou G, Kennedy DN, Hodge SM, Moore CM, Howard JD, Rohan MP, Caviness VS, Makris N. White matter abnormalities in children with and at risk for bipolar disorder. Bipolar Disorders. 2007; 9:799–809. [PubMed: 18076529]

Gao W, Jiao Q, Qi R, Zhong Y, Lu D, Xiao Q, Lu S, Xu C, Zhang Y, Liu X. Combined analyses of gray matter voxel-based morphometry and white matter tract-based spatial statistics in pediatric bipolar mania. Journal of Affective Disorders. 2013; 150:70–76. [PubMed: 23477846]

Goldstein TR, Birmaher B, Axelson D, Ryan ND, Strober MA, Gill MK, Valeri S, Chiappetta L, Leonard H, Hunt J. History of suicide attempts in pediatric bipolar disorder: factors associated with increased risk. Bipolar Disorders. 2005; 7:525–535. [PubMed: 16403178]

Gönenç A, Frazier JA, Crowley DJ, Moore CM. Combined diffusion tensor imaging and transverse relaxometry in early-onset bipolar disorder. Journal of the American Academy of Child & Adolescent Psychiatry. 2010; 49:1260–1268. [PubMed: 21093775]

Harmon-Jones E, Abramson LY, Nusslock R, Sigelman JD, Urosevic S, Turonie LD, Alloy LB, Fearn M. Effect of bipolar disorder on left frontal cortical responses to goals differing in valence and task difficulty. Biological Psychiatry. 2008; 63:693–698. [PubMed: 17919457]

Hasan KM, Walimuni IS, Abid H, Datta S, Wolinsky JS, Narayana PA. Human brain atlas-based multimodal MRI analysis of volumetry, diffusimetry, relaxometry and lesion distribution in multiple sclerosis patients and healthy adult controls: implications for understanding the pathogenesis of multiple sclerosis and consolidation of quantitative MRI results in MS. Journal of the Neurological Sciences. 2012; 313:99–109. [PubMed: 21978603]

Hasan KM, Walimuni IS, Abid H, Frye RE, Ewing-Cobbs L, Wolinsky JS, Narayana PA. Multimodal quantitative magnetic resonance imaging of thalamic development and aging across the human lifespan: implications to neurodegeneration in multiple sclerosis. Journal of Neuroscience. 2011; 31:16826–16832. [PubMed: 22090508]

Hein G, Knight R. Superior temporal sulcus—it's my area: or is it? Journal of Cognitive Neuroscience. 2008; 20:2125–2136. [PubMed: 18457502]

James A, Hough M, James S, Burge L, Winmill L, Nijhawan S, Matthews PM, Zarei M. Structural brain and neuropsychometric changes associated with pediatric bipolar disorder with psychosis. Bipolar Disorders. 2011; 13:16–27. [PubMed: 21320249]

Johansen-Berg, H.; Behrens, TE. Diffusion MRI: From Quantitative Measurement to In Vivo Neuroanatomy. Academic Press; San Diego: 2013.

Johnston B, Mwangi B, Matthews K, Coghill D, Steele J. Predictive classification of individual magnetic resonance imaging scans from children and adolescents. European Child & Adolescent Psychiatry. 2013; 22:733–744. [PubMed: 22930323]

Johnston BA, Mwangi B, Matthews K, Coghill D, Konrad K, Steele JD. Brainstem abnormalities in attention deficit hyperactivity disorder support high accuracy individual diagnostic classification. Human Brain Mapping. 2014; 35:5179–5189. [PubMed: 24819333]

Jonas BS, Brody D, Roper M, Narrow WE. Prevalence of mood disorders in a national sample of young American adults. Social Psychiatry and Psychiatric Epidemiology. 2003; 38:618–624. [PubMed: 14614549]

Klöppel S, Abdulkadir A, Jack CR, Koutsouleris N, Mourão-Miranda J, Vemuri P. Diagnostic neuroimaging across diseases. Neuroimage. 2012; 61:457–463. [PubMed: 22094642]

Kochunov P, Williamson D, Lancaster J, Fox P, Cornell J, Blangero J, Glahn D. Fractional anisotropy of water diffusion in cerebral white matter across the lifespan. Neurobiology of Aging. 2012; 33:9–20. [PubMed: 20122755]

Kriegeskorte N, Simmons WK, Bellgowan PS, Baker CI. Circular analysis in systems neuroscience: the dangers of double dipping. Nature Neuroscience. 2009; 12:535–540. [PubMed: 19396166]

Krystal JH, State MW. Psychiatric disorders: diagnosis to therapy. Cell. 2014; 157:201–214. [PubMed: 24679536]

Kupfer DJ. The increasing medical burden in bipolar disorder. JAMA. 2005; 293:2528–2530. [PubMed: 15914754]

Merikangas KR, Cui L, Kattan G, Carlson GA, Youngstrom EA, Angst J. Mania with and without depression in a community sample of US adolescents. Archives of General Psychiatry. 2012; 69:943–951. [PubMed: 22566563]

Misaki M, Kim Y, Bandettini PA, Kriegeskorte N. Comparison of multivariate classifiers and response normalizations for pattern-information fMRI. Neuroimage. 2010; 53:103–118. [PubMed: 20580933]

Mori S, Itoh R, Zhang J, Kaufmann WE, van Zijl P, Solaiyappan M, Yarowsky P. Diffusion tensor imaging of the developing mouse brain. Magnetic Resonance in Medicine. 2001; 46:18–23. [PubMed: 11443706]

Mori S, Zhang J. Principles of diffusion tensor imaging and its applications to basic neuroscience research. Neuron. 2006; 51:527–539. [PubMed: 16950152]

Mwangi B, Ebmeier KP, Matthews K, Steele JD. Multi-centre diagnostic classification of individual structural neuroimaging scans from patients with major depressive disorder. Brain. 2012; 135:1508–1521. [PubMed: 22544901]

Mwangi B, Hasan KM, Soares JC. Prediction of individual subject's age across the human lifespan using diffusion tensor imaging: a machine learning approach. Neuroimage. 2013; 75:58–67. [PubMed: 23501046]

Mwangi B, Spiker D, Zunta-Soares GB, Soares JC. Prediction of pediatric bipolar disorder using neuroanatomical signatures of the amygdala. Bipolar Disorders. 2014a; 16:713–721. [PubMed: 24917530]

Mwangi B, Tian TS, Soares JC. A review of feature reduction techniques in neuroimaging. Neuroinformatics. 2014b; 12:229–244. [PubMed: 24013948]

Orrù G, Pettersson-Yeo W, Marquand AF, Sartori G, Mechelli A. Using support vector machine to identify imaging biomarkers of neurological and psychiatric disease: a critical review. Neuroscience & Biobehavioral Reviews. 2012; 36:1140–1152. [PubMed: 22305994]

Passarotti AM, Sweeney JA, Pavuluri MN. Emotion processing influences working memory circuits in pediatric bipolar disorder and attention-deficit/hyperactivity disorder. Journal of the American Academy of Child & Adolescent Psychiatry. 2010; 49:1064–1080. [PubMed: 20855051]

Pavuluri MN, O`Connor MM, Harral E, Sweeney JA. Affective neural circuitry during facial emotion processing in pediatric bipolar disorder. Biological Psychiatry. 2007; 62:158–167. [PubMed: 17097071]

Pierpaoli C, Jezzard P, Basser PJ, Barnett A, Di Chiro G. Diffusion tensor MR imaging of the human brain. Radiology. 1996; 201:637–648. [PubMed: 8939209]

Post RM, Leverich GS, Kupka RW, Keck PE Jr, McElroy SL, Altshuler LL, Frye MA, Luckenbaugh DA, Rowe M, Grunze H. Early-onset bipolar disorder and treatment delay are risk factors for poor outcome in adulthood. Journal of Clinical Psychiatry. 2010; 71:864. [PubMed: 20667291]

Salat DH, Greve DN, Pacheco JL, Quinn BT, Helmer KG, Buckner RL, Fischl B. Regional white matter volume differences in nondemented aging and Alzheimer's disease. Neuroimage. 2009; 44:1247–1258. [PubMed: 19027860]

Schwaighofer A. Support Vector Machine Matlab Toolbox. Matlab, Natick, MA. Smith, S.M., 2002. Fast robust automated brain extraction. Human Brain Mapping. 2001; 17:143–155.

Song S-K, Sun S-W, Ju W-K, Lin S-J, Cross AH, Neufeld AH. Diffusion tensor imaging detects and differentiates axon and myelin degeneration in mouse optic nerve after retinal ischemia. Neuroimage. 2003; 20:1714–1722. [PubMed: 14642481]

Song S-K, Sun S-W, Ramsbottom MJ, Chang C, Russell J, Cross AH. Dysmyelination revealed through MRI as increased radial (but unchanged axial) diffusion of water. Neuroimage. 2002; 17:1429–1436. [PubMed: 12414282]

Stoddard J, Hsu D, Reynolds RC, Brotman MA, Ernst M, Pine DS, Leibenluft E, Dickstein DP. Aberrant amygdala intrinsic functional connectivity distinguishes youths with bipolar disorder from those with severe mood dysregulation. Psychiatry Research: Neuroimaging. 2015; 231(2): 120–125. [PubMed: 25544024]

Tamnes CK, Østby Y, Fjell AM, Westlye LT, Due-Tønnessen P, Walhovd KB. Brain maturation in adolescence and young adulthood: regional age-related changes in cortical thickness and white matter volume and microstructure. Cerebral Cortex. 2010; 20:534–548. [PubMed: 19520764]

Vapnik, V. Statistical Learning Theory. Wiley; New York: 1998.

Wu M-J, Wu H, Mwangi B, Sanches M, Selvaraj S, Zunta-Soares GB, Soares JC. Prediction of pediatric unipolar depression using multiple neuromorphometric measurements: a pattern classification approach. Journal of Psychiatric Research. 2015; 62:84–91. [PubMed: 25687738]

Highlights

- Support vector machines and DTI scans are used to predict individual PBD patients
- Support vector machines predict PBD patients with above chance level sensitivity and specificity.
- Patterns of reduced fractional anisotropy were `most relevant' in distinguishing PBD patients from Healthy controls.

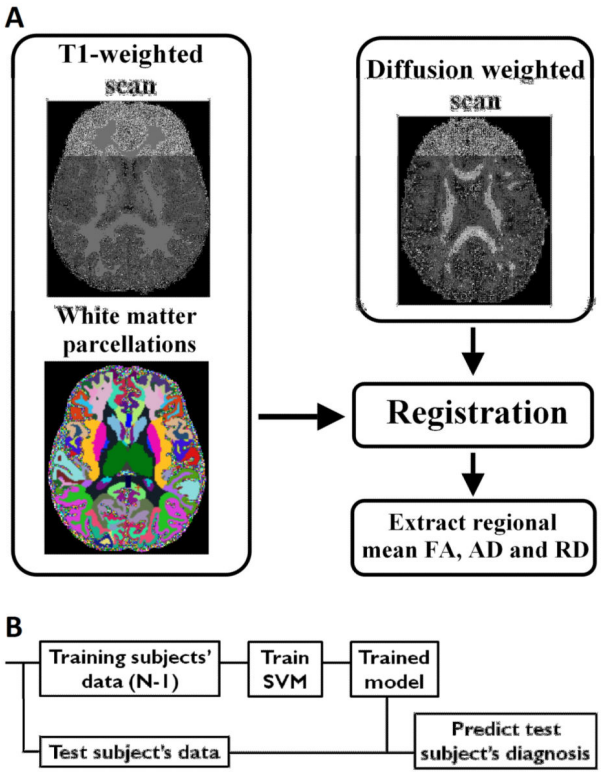

Fig. 1.

A) Flow diagram illustrating the multi-modal (T1-weighted and DWI) co-registration and regional feature extraction process. The FLIRT image registration routine was utilized with FA and Freesurfer white matter parcellations as `source' and `target' volumes respectively. Regional FA, AD and RD values were extracted and used as input data in the SVM analyses. **Fig. 1. B)** An illustration of the LOOCV approach which was used in `training' and `testing' the SVM algorithm.

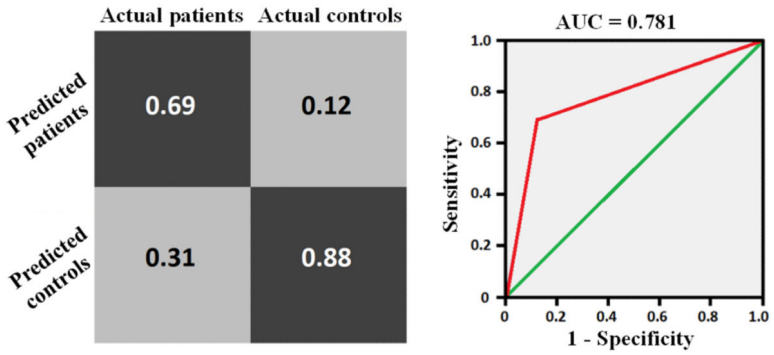

Fig. 2.

A `confusion matrix' and receiver operating characteristic curve used to evaluate linear SVM model performance. Accuracy =78.12 %, specificity =87.5 %, sensitivity =68.75 %, positive predictive value =84.62 %, negative predictive value = 73.68%, chi-square *p*-value =0.0012 and AUROC = 0.7812.

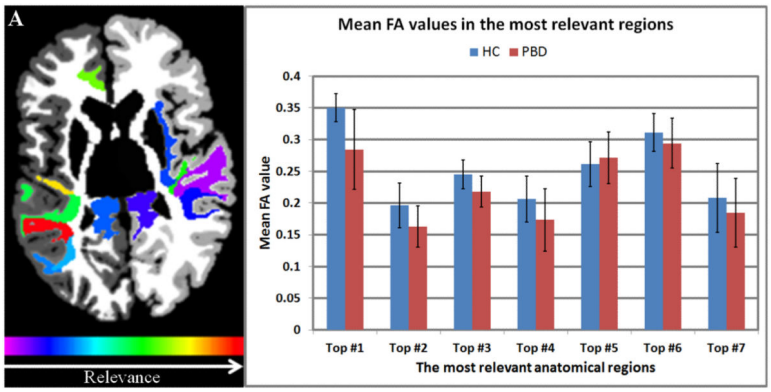

Fig. 3.

A) Illustration of anatomical regions identified by SVM as `most relevant' in distinguishing PBD patients from healthy controls. **Fig. 3. B)** A graphical illustration of top 7 `most relevant' anatomical regions. Top #1 – left banks of superior temporal sulcus, Top #2 – left frontal pole, Top #3 – left Parahippocampal gyrus, Top #4 – left transverse temporal gyrus, Top #5- right temporal pole, Top #6 – left rostral anterior cingulate, Top #7 – right transverse temporal gyrus.

Table 1

Demographic and clinical details

Characteristic	Bipolar patients Mean(SD)	Healthy controls Mean(SD)	Analysis		
			F/χ^2	df	*p*
Age (years)	12.24 (3.31)	12.42 (3.06)	$F = 0.03$	30	$P=0.87$
Sex (females/total)	6/16	6/16	$\chi^2= 0$	1	$P=1.0$
Years of education	5.38 (3.18)	6.25 (3.30)	$F = 0.58$	30	$P=0.45$
YMRS	7.19 (4.74)	0.38 (0.62)	$F = 32.55$	30	$P<0.0001$
CDRS	27.00 (9.49)	17.75 (1.34)	$F = 10.22$	28**	$P=0.0045$
Ethnicity	Non-Hispanic White- 16 Hispanic- 0 Other- 0	Non-Hispanic White- 14 Hispanic-2 Other- 0	$\chi^2 = 2.13$	1	$P=0.14$
Petersen development scores	2.23 (0.85)	2.36 (1.05)	$F = 0.09$	28**	$P=0.76$
Handedness	1 (0.73)	1.07 (0.54)	$\chi^2 = 1.327$	1	$P=0.28$
Illness duration	35 (30.28)*	-	-	-	-
Bipolar type	BP-I 2/16 BP-II 4/16 BP-NOS 10/16	-	-	-	-
Comorbidities	ADHD- 10 ODD-7 Adjustment disorder- 1 Panic disorder w/ Agoraphobia- 1 Specific phobia- 1 Separation anxiety- 1 Enuresis- 4 Encopresis- 1 GAD- 1	-	-	-	-

F- F statistic, χ^2 – chi-square test, df – degrees of freedom, ADHD-attention deficit-hyperactivity disorder, ODD-oppositional defiant disorder, GAD-generalized anxiety disorder.

* Illness duration presented in months,

** two subjects with missing values,

Table 2

Summary of SVM prediction results using a linear kernel

DTI feature	Accuracy	Sensitivity	Specificity	PPV	NPV	AUROC	χ^2	*p*-value
FA	78.12%	68.75%	87.50%	84.62%	73.68%	0.7812	10.49	0.0012*
AD	59.38%	37.50%	81.25%	66.67%	56.52%	0.5938	1.39	0.2382
RD	56.25%	56.25%	56.25%	56.25%	56.25%	0.5625	0.5	0.4795

PPV- positive predictive value, NPV- negative predictive value, AUROC-area under receiver operating characteristic curve.

* chi-square *p*-value significant ($p<0.05$).

Table 3

A list of most relevant regions in distinguishing PBD patients from healthy controls.

SVM relevance ranking	Anatomical region
1	Left banks of the superior temporal sulcus
2	Left frontal pole
3	Left parahippocampal gyrus
4	Left transverse temporal gyrus
5	Right temporal pole
6	Left anterior cingulate gyrus
7	Right transverse temporal gyrus
8	Left superior temporal gyrus
9	Right parahippocampal gyrus
10	Left paracentral lobule
11	Left inferior parietal lobule
12	Left isthmus of left cingulate gyrus
13	Left posterior part of left middle frontal gyrus
14	Right inferior temporal gyrus
15	Right superior temporal gyrus